

Improvement of vibration energy harvesters mechanical Q-factor through high density proof mass integration

A Dompierre^{1,2} and L G Fréchette^{1,2}

¹Institut Interdisciplinaire d'Innovation Technologique (3IT), 3IT.nano, Université de Sherbrooke, Sherbrooke, QC, J1K 0A5, Canada

²Laboratoire de Nanotechnologie et Nanosystème (LN2), CNRS UMI-3463, Université de Sherbrooke, Sherbrooke, QC, J1K 0A5, Canada

andre.dompierre@usherbrooke.ca

Abstract. This paper reports on improvement of the mechanical Q-factor of resonant energy harvesters at ambient pressure via the use of tungsten proof masses by evaluating the impact of the mass size and density on the squeeze film damping. To this end, a simplified model is first proposed to evaluate cantilever beams deflection and the resulting fluid pressure build up between the mass and a near surface. The model, which accounts for simultaneous transverse and rotational motion of very long tip masses as well as for 2D fluid flow in the gap, is used to extract a scaling law for the device fluidic Q-factor Q_f . This law states that Q_f can be improved by either increasing the linear mass density of the tip mass or by reducing the side lengths compared to the gap height. The first approach is validated experimentally by adding a tungsten proof mass on a silicon based device and observing an improvement of the Q-factor by 103%, going from 430 to 871, while the resonance frequency drops from 457 to 127 Hz. In terms of fluidic Q-factor, this represents an increase from 562 to 1673. These results successfully demonstrate the benefits of integrating a tungsten mass to reduce the fluid losses while potentially reducing the device footprint.

1. Introduction

As demonstrated by previous research [1], energy losses due to fluidic damping can substantially reduce the performance of MEMS vibration energy harvesters in ambient pressure. Unpackaged devices are typically subject to viscous friction with air, while squeeze film damping is observed in packaged harvesters due to fluid confinement in the cavity [1,2]. The latter actually leads to worse performance in terms of damping and efficiency, but packaging is nonetheless necessary to protect the fragile structure. The typical solution to this issue is to use a vacuum sealed package [1,3], but hermiticity now becomes a new concern. The mass can also be perforated to improve fluid circulation, although it comes at the expense of its effective density.

High density materials improve the power density of vibration energy harvesters due to an increased sensitivity to input vibrations [4,5]. In this paper, we furthermore highlight how their integration can also be an effective way to reduce the effects of fluidic damping on the device mechanical Q-factor. We first propose a simplified model to analytically verify the impact of a mass density variation from silicon (Si) to tungsten (W) on squeeze film damping. This effect is then shown



experimentally by characterization of the Q-factor of Si-AlN based piezoelectric microcantilevers fabricated using MEMSCAP's PiezoMUMPs process.

2. Beam and fluid damping modelling

2.1. General assumptions and definitions

Several factors affect the interaction of the harvester with the surrounding fluid. For this work, we assume isothermal conditions, ideal venting ($P=0$ at the boundaries), small displacement and that air is an ideal gas. The variables are therefore the ambient pressure P_a , geometry and frequency ω .

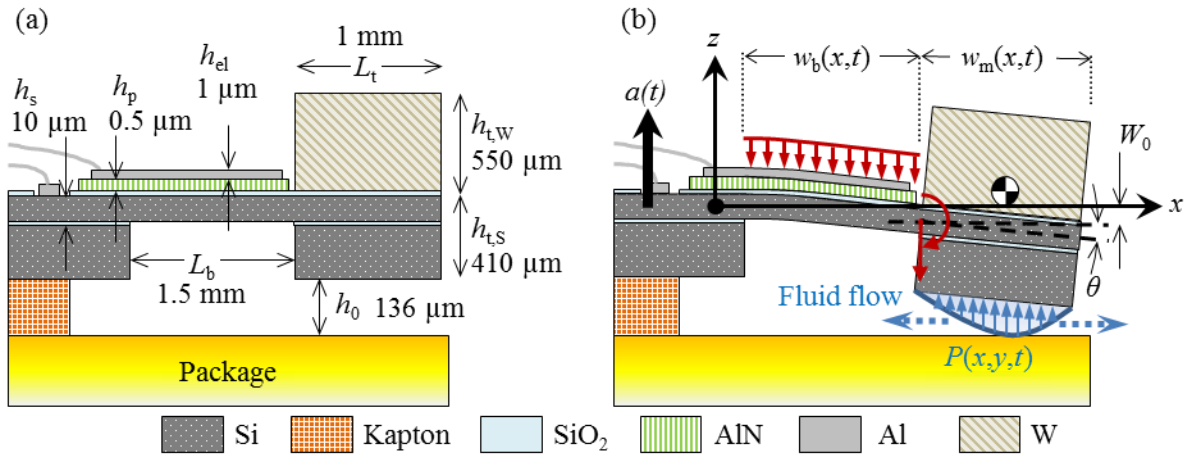


Figure 1. Diagram of the packaged piezoelectric cantilevers, unstrained with the dimensions (a) and deflected under the combined load with the squeeze film pressure in the gap (b).

The configuration of the packaged piezoelectric cantilevers studied is depicted in figure 1. The first mode of the beam $\hat{w}_b(x)$, excited by the harmonic base acceleration $a(t)$, is approximated to the static deflection of a cantilever subject to a combined load. The inertia of the beam of length L_b and width b is considered as a constant distributed load while the tip mass applies a punctual force and a moment to the tip of the cantilever. The tip mass rotary inertia is also assumed negligible. The beam deflection $w_b(x,t)$, defined over the domain $x=[0, L_b]$, can therefore be expressed as in equation (2.1) [6]

$$w_b(x,t) = \hat{w}_b(x)W_0 \sin(\omega t) = \frac{\left[6 + 12\lambda\left(\frac{L_t}{L_b} + \frac{1}{2}\left(\frac{L_t}{L_b}\right)^2\right)\right]\left(\frac{x}{L_b}\right)^2 - 4\left(1 + \lambda\frac{L_t}{L_b}\right)\left(\frac{x}{L_b}\right)^3 + \left(\frac{x}{L_b}\right)^4}{3 + 8\lambda\frac{L_t}{L_b} + 6\lambda\left(\frac{L_t}{L_b}\right)^2} \sin(\omega t) \quad (2.1)$$

where W_0 is the beam tip amplitude, L_t is the length of the proof mass and λ is the ratio of the linear mass density of the proof mass to the beam which depends on the material's densities ρ and thicknesses h ,

$$\lambda = (\rho_s h_{t,s} + \rho_w h_{t,w}) / (\rho_s h_s + \rho_p h_p + \rho_{el} h_{el}). \quad (2.2)$$

The displacement of the mass $w_m(x,t)$, defined over $x=[L_b, L_b+L_t]$, is then the combined result of the beam tip transverse motion W_0 and rotation due to the tip angle θ . Noting $\hat{\theta} \approx d\hat{w}_b(L_b)/dx$ as the normalized tilt angle,

$$w_m(x,t) = \left[1 + (x - L_b)\hat{\theta}\right]W_0 \sin(\omega t). \quad (2.3)$$

Equation (2.4) finally provides the definition of the Q-factor,

$$Q_{\text{tot}} = (Q_{\text{int}}^{-1} + Q_{\text{f}}^{-1})^{-1} = 2\pi \frac{\text{Stored Energy}}{\text{Dissipated Energy per Cycle}} = \pi M_{\text{eq}} \omega^2 W_0^2 / U_D, \quad (2.4)$$

where Q_{int} and Q_{f} are respectively the intrinsic and fluidic Q-factor. Meanwhile, U_D is obtained by integrating over the structure area and over one period the product of the local drag force induced by

the pressure field $P(x,y,t)$ with the local velocity $\dot{w}(x,t)$. The problem therefore lies in properly evaluating the distribution of this force. This section quickly presents the basic model for 2D squeeze film flow to showcase the impact of the tip mass density and its geometry.

2.2. Squeeze film damping

Due to the fluid flow restriction in the tight h_0 thick gap between the mass and the package, squeeze film damping will only occur in this area. The linearized differential equation of the normalized pressure field P^* for a compressible 2D squeeze film is described by the classic Reynolds equation [7]

$$\frac{\partial^2 P^*}{\partial x^2} + \frac{\partial^2 P^*}{\partial y^2} - \frac{12\mu_{\text{eff}}}{h_0^2 P_a} \frac{\partial P^*}{\partial t} = -\frac{12\mu_{\text{eff}}}{h_0^2 P_a} \frac{\partial \tilde{h}(x,t)}{\partial t} \quad (2.5)$$

with \tilde{h} the normalized gap function given by equation (2.6)

$$\tilde{h}(x,t) = 1 - w_m(x,t)/h_0. \quad (2.6)$$

Equation (2.5) is solved using the approach presented in [8] which yields equation (2.7), the pressure field expressed as a sum of eigenmodes

$$P(x,y,t) = P_a \frac{W_0}{h_0} \tilde{P}(x,y) \cos(\omega t) = P_a \frac{W_0}{h_0} \sum_{mn} \phi_{mn} C_m C_n \cos\left(\frac{m\pi(x-L_b)}{L_t} - \frac{m\pi}{2}\right) \cos\left(\frac{n\pi y}{b}\right) \cos(\omega t), \quad (2.7)$$

where cos and sin are respectively used for odd and even indices m, n while C_m, C_n and ϕ_{mn} are computed from equations (2.8) and (2.9).

$$\phi_{mn} = \frac{\sigma_{mn}}{1 + j\sigma_{mn}}, \quad C_m = \begin{cases} \frac{2(L_t\theta+2)}{\pi n} (-1)^{\frac{(m-1)}{2}} \\ \frac{2L_t\theta}{\pi n} (-1)^{\frac{m}{2}+1} \end{cases}, \quad C_n = \begin{cases} \frac{4}{n\pi} (-1)^{\frac{(n-1)}{2}} & \text{odd} \\ 0 & \text{even} \end{cases} \quad (2.8)$$

$$\sigma_{mn} = \frac{12\mu_{\text{eff}}\omega}{h_0^2 P_a} \left[\pi^2 \left(\frac{m^2}{L_t^2} + \frac{n^2}{b^2} \right) \right]^{-1} \quad (2.9)$$

Here σ_{mn} are equivalent to modal squeeze numbers. For large σ_{mn} , the fluid is compressible and contributes to an increased stiffness. Conversely, the pressure field is mainly dissipative for smaller σ_{mn} which should be the case here ($\sigma_{11} \approx 5\text{E-}6$ at 1 atm) and therefore $\text{Re}[P] \approx P$. The energy dissipated, U_D , is derived in equation (2.10) by integrating the pressure field over the mass surface and one period,

$$U_D = \int_{L_b}^{L_b+L_t} \int_{-b/2}^{b/2} \int_0^{2\pi/\omega} P(x,y,t) \dot{w}_m(x,t) dt dy dx = W_0^2 \frac{P_a}{h_0} \int_{L_b}^{L_b+L_t} \int_{-b/2}^{b/2} \tilde{P}(x,y) [1 + (x-L_b)\hat{\theta}] dy dx. \quad (2.10)$$

Replacing U_D in equation (2.4) by equation (2.10) finally yields the fluidic Q-factor,

$$Q_f = M_{\text{eq}} \omega^2 h_0 \left(P_a \int_{L_b}^{L_b+L_t} \int_{-b/2}^{b/2} \tilde{P}(x,y) [1 + (x-L_b)\hat{\theta}] dy dx \right)^{-1} \quad (2.11)$$

An exact simplified expression for Q_f that covers all geometry range is not straightforward to obtain, but we can nonetheless extract a general trend by developing equation 2.11 for the case of a sizeable tip mass. Upon simplification, this trends is expressed as equation (2.12),

$$Q_f \propto \frac{\omega(\rho_l h_l b)}{\mu_{\text{eff}}} \left(\frac{h_0}{l} \right)^3, \quad (2.12)$$

where l is the smallest planar feature size of the mass. The first term therefore states that Q_f will improve proportionally with the linear mass density. This is either done by increasing the material density, as we propose here, or by increasing the thickness. This second option may however reduce the gap h_0 if the space is constrained. Meanwhile, the second term is affected by a cubic power and shows potential for drastic improvement if the gap to side length ratio is increased.

3. Case study application and experimental validation

3.1. Experimental setup and procedure

The piezoelectric devices, shown on figure 2, were fabricated via MEMSCAP's PiezoMUMPs process. The process uses a n-type SOI wafer as the starting substrate with a 10 μm thick device layer and 400 μm handle layer. The device layer acts as the beam support material and is phosphorous doped to also serve as the bottom electrode. The piezoelectric layer consists of 0.5 μm thick sputtered AlN and the top electrode is a metal stack of 20 nm Cr and 1 μm thick Al defined by lift-off. The beam and mass geometries are machined by DRIE through the device and handle layer respectively.

The nominal width of the beam and mass of the tested design is 1 mm while the other dimensions are illustrated in figure 1(a). A shaker setup was used to excite the cantilever at its resonance frequency and was suddenly turned off to measure the decay time. A first measurement was done with the Si proof mass ($\rho_s=2.33 \text{ g/cm}^3$) in vacuum ($P_a=5\text{E-}4 \text{ mbar}$) to evaluate Q_{int} and a second one was conducted at atmospheric pressure to evaluate Q_{tot} and extract Q_f from equation (2.4). A W mass ($\rho_w=19.3 \text{ g/cm}^3$) was subsequently glued on top of the Si mass and the same methodology was repeated. The displacement was measured via the piezoelectric open circuit voltage and the Q-factors were computed via the logarithmic decrement method using a curve fitting algorithm. Four waveforms were recorded and analyzed for each condition.

3.2. Results and discussion

The results of the simulation (max $m, n=10$) are compared with our experiments in table 1 and show good agreement despite some of the nonlinearities observed. As anticipated, the tungsten mass reduces the resonance frequency ω_n significantly from 457.49 Hz to 126.27 Hz while a 103% increase of Q_{tot} is observed. The model follows the same trends, although with a small offset which could be explained by errors on the dimensions or by residual stresses (the value of Q_f is especially sensitive to h_0). Acknowledging for the measured Q_{int} , the derived Q_f shows a 3 fold increase which is expected considering the frequency drop (see equation 2.12). For comparison's sake, we also considered an additional modelling scenario where the mass length is adjusted to conserve the frequency. A significant reduction of fluid damping is again observed. However, viscous flow would probably more aptly represent this scenario considering the reduction of h_0/L_t . These results successfully demonstrate the benefits of integrating a tungsten mass to simultaneously reduce the footprint and the fluid losses.

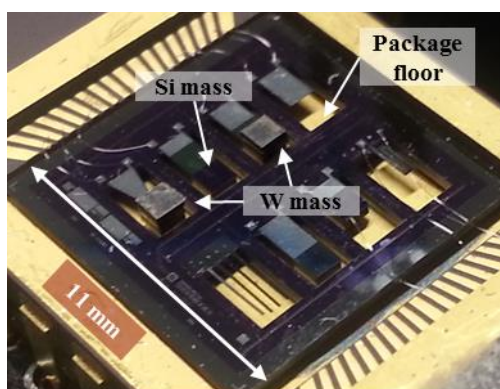


Figure 2. Close up view of a PiezoMUMPs die, featuring designs with silicon and glued tungsten masses.

Table 1. Simulation and experimental results

		ω_n^a (Hz)	Q_{int}	Q_{tot}^a	Q_f^a
Exp	Si	457.49	1836	430	562
	Si + W	126.27	1817	871	1673
Model	Si	483.18	1825	437	575
	Si + W	136.68	1825	962	2033
	Si + W ^b	484.18	1825	1812	5E5

^a at 1 atm

^b $L_t = 106 \mu\text{m}$

4. Conclusion

We have successfully shown analytically and experimentally the impact of the tip mass density and geometry on the fluidic damping and device Q-factor. A simplified analytical model was first

introduced to describe the 2D squeeze film and the beam behaviour. The model mainly shows that Q_f can be improved by increasing the linear mass density, by using tungsten instead of silicon for instance, or by reducing the mass area if the frequency is fixed. The first approach was verified experimentally and has shown that it is possible to double the total Q-factor at ambient pressure. Beside the improvement in efficiency, the harvester also benefits from an improved sensitivity to input vibration which can drastically improve its power density.

5. References

- [1] Elfrink R, *et al.* 2010 Vacuum-packaged piezoelectric vibration energy harvesters: damping contributions and autonomy for a wireless sensor system *J. Micromech. Microeng.* **20** 104001
- [2] Hosaka H, Ito K and Kuroda S 1995 Damping characteristics of beam-shaped micro-oscillators *Sensors and Actuators A* **49** 87–95
- [3] Aktakka E E and Najafi K 2014 A micro inertial energy harvesting platform with self-supplied power management circuit for autonomous wireless sensor nodes *IEEE J. of Solid-State Circuits* **49** 2017–29
- [4] Mitcheson P D, Green T C, Yeatman E M and Holmes A S 2004 Architectures for vibration-driven micropower generators *J. Microelectromech. Syst.* **13** 429–40
- [5] Dompierre A, Vengallatore S and Fréchet L G 2011 Theoretical and practical limits of power density for piezoelectric vibration energy harvesters *Proc. of PowerMEMS 2011 (Seoul)* 249–52
- [6] Bazergui A, Bui-Quoc T, Biron A, McIntyre G and Laberge C 2002 *Résistance des Matériaux, troisième édition* (Montreal: Presses Internationales Polytechnique) chapter 5 p 118
- [7] Bao M and Yang H 2007 Squeeze film air damping in MEMS *Sensors and Actuators A* **136** 3–27
- [8] Darling R B, Hivick C and Xu J 1998 Compact analytical modeling of squeeze film damping with arbitrary venting conditions using a Green's function approach *Sensors and Actuators A* **70** 32–41

Acknowledgment

We would like to acknowledge the financial support of NSERC and the technical support of the 3IT staff members. We'd especially like to thank Daniel Blackburn for his help in setting up the vacuum chamber used in these tests.